MDC 93H1355
JUNE 1993

MIRROR FUSION PROPULSION SYSTEM: A PERFORMANCE COMPARISON WITH ALTERNATE PROPULSION SYSTEMS FOR THE MANNED MARS MISSION

M. DEVENY
McDonnell Douglas Aerospace
S. CARPENTER
Lawrence Berkeley Laboratory
T. O'CONNELL
Independent
N. SCHULZE
NASA Headquarters

Presented to
AIAA/SAE/ASME/ASEE
29th Joint Propulsion
Conference and Exhibit
Monterey, California
28–30 June 1993

McDonnell Douglas Aerospace
Space Systems

MCDONNELL DOUGLAS

MIRROR FUSION PROPULSION SYSTEM: A PERFORMANCE COMPARISON WITH ALTERNATE PROPULSION SYSTEMS FOR THE MANNED MARS MISSION

M. Deveny*
McDonnell Douglas Aerospace
Huntington Beach, California

S. Carpenter†
Lawrence Berkeley Laboratory
Berkeley, California

T. O'Connell**
Independent
Placentia, CA

N. Schulze††
NASA Headquarters
Washington D.C.

Abstract

The performance characteristics of several propulsion technologies applied to piloted Mars missions are compared. The characteristics that are compared are Initial Mass in Low Earth Orbit (IMLEO), mission flexibility, and flight times. The propulsion systems being compared are both demonstrated and envisioned: Chemical (or Cryogenic), Nuclear Thermal Rocket (NTR) solid core, NTR gas core, Nuclear Electric Propulsion (NEP), and a mirror fusion space propulsion system. The proposed magnetic mirror fusion reactor, known as the Mirror Fusion Propulsion System (MFPS), is described. The description is an overview of a design study that was conducted to convert a mirror reactor experiment at Lawrence Livermore National Lab (LLNL) into a viable space propulsion system. Design principles geared towards minimizing mass and maximizing power available for thrust are identified and applied to the LLNL reactor design, resulting in the MFPS. The MFPS' design evolution, reactor and fuel choices, and system configuration are described. Results of the performance comparison shows that the MFPS minimizes flight time to 60 to 90 days for flights to Mars while allowing continuous return-home capability while at Mars. Total MFPS IMLEO including propellant and payloads is kept to about 1,000 metric tons.

* Engineer/Scientist Specialist, Member, AIAA
† Senior Research Associate, Earth Sciences Division.
** Aerospace Engineer
†† Aerospace Engineer, Flight Systems

Nomenclature

B	magnetic field strength
g	local gravitational acceleration
G	gravitational acceleration at Earth's surface
Isp	specific impulse
P_{AFT}	power available for thrust
P_{Brem}	Bremsstrahlung radiation power
P_{FUS}	total fusion power
P_n	neutron power
P_{syn}	synchrotron radiation power
P_C	plasma transport power
Q	reactor energy gain
Z	atomic number
υ	angle travelled about the Sun during flight

Introduction

Crew safety and recurring mission cost are probably the two greatest drivers in the design of a piloted Mars mission[1].

Crew safety is affected by exposure to the space environment. Exposure of the crew to the space environment includes solar radiation, galactic cosmic radiation, and zero gravity. Spinning a spacecraft may not be desireable due to vehicle design complexity, and it may not prevent the crew's loss of muscle and bone mass in any event. Radiation shielding may not prevent secondary radiation from emanating from the bombardment of structures by cosmic galactic radiation, from reaching the crew. Minimizing flight time is the only known means to reduce both the threat of zero gravity and radiation.

The other major factor affecting crew safety is mission flexibility. In the event of a failure or crippling of a crew-critical subsystem that results in the

subsystem's not being able to support the crew for the full length of a mission, then the mission would have to be cut short. It would be desireable - though not possible for most propulsion systems - to have the ability to begin the trip home at any time.

One of the largest components of recurring cost will be launch costs. If a Heavy-Lift Launch Vehicle (HLLV) is developed with the capability to place approximately 150,000 kg[1] in Low Earth Orbit (LEO), then anywhere from five to ten HLLVs would be needed for each piloted mission. Therefore, the Initial Mass in Low Earth Orbit (IMLEO) of any potential Mars Transportation System must be minimized.

In this paper we will compare the following three mission performance parameters:

1) IMLEO,
2) flight time to Mars, and
3) mission flexibility,

for the following five propulsion systems:

1) Chemical (cryogenic),
2) Nuclear Thermal Rocket (NTR) solid core,
3) Nuclear Thermal Rocket (NTR) gas core,
4) Nuclear Electric Propulsion (NEP) at varying power levels, and
5) A proposed magnetic-containment fusion engine known as the Mirror Fusion Propulsion System (MFPS)[2].

Before comparing these systems and their capabilities, we will discuss the MFPS design and background due to its being relatively unknown compared to the other propulsion systems. This discussion is an overview of a design study done earlier[2]. Discussion will include rationale behind the choice of fusion ractor configuration and fusion fuel to be used for MFPS, mirror fusion evolution, design drivers of the MFPS to minimize mass and maximize available power, and finally, an overview of the MFPS subsystems and configuration. We will show that this unique approach to fusion propulsion may result in a feasible fusion engine with superior mission performance capabilities.

Part 1: The Choice of Reactor Configuration and Fuel for Space Propulsion
Part 2: Design Principles for Space Fusion Propulsion
Part 3: Mirror Fusion Propulsion System (MFPS) Design Overview
Part 4: The Performance Comparison of MFPS With Alternative Propulsion Systems

Part 1
The Choice of Reactor Configuration and Fuel for Space Propulsion

The choices of fusion reactor configuration and fuel to be used are by far the most important parameters for defining the performance of a fusion space propulsion system.

Fusion Reactors

To summarize the configurations available, there are two basic approaches to controlling fusion: magnetic confinement fusion (MCF) and inertial confinement fusion (ICF). MCF operates through the containment and heating of the fuel as a tenuous plasma to achieve ignition using a powerful magnetic field. ICF operates by implosion of the fuel in the form of pellets to achieve ignition, using particle or laser beams.

In MCF reactors, the plasma ions are trapped on the magnetic field lines, keep enough fuel particles together for fusion to occur. MCF reactors fall into two main classes: "closed" and "open." Each of these two classes entails great diversity; but there is one fundamental difference. In the closed class (see Figure 1), the magnetic field lines and plasma remain trapped inside a mechanical device (the fusion reactor) whereas in the open class (see example in Figure 2a), the magnetic field lines and the charged particle fusion products are allowed to escape beyond the confines of the physical reactor. Thus, as a propulsion system, the open-class MCF allows for greater system efficiency because the fusion products can be applied directly to thrust.

Fusion Fuels

To take advantage of the opportunity offered by the open-class MCF reactor to allow charged particles to heat a propellant directly, a combination of fuels must be found that produces the greatest possible amount of charged particles. The fuel candidates can be found among the isotopes of hydrogen and helium.

Nuclear fusion is the process that combines very light atomic nuclei; such as hydrogen-2 (deuterium), hydrogen-3 (tritium) and helium-3, to release nucleon binding energy. The reaction of deuterium with tritium (DT) is written as (energy in MeV):

$$ {}^{2}_{1}D_{(0.02)} + {}^{3}_{1}T_{(0.02)} \rightarrow {}^{1}_{0}n_{(14.07+0.032)} + {}^{4}_{2}He_{(3.52+0.008)} , $$

which releases about 80% of the energy produced as neutron kinetic energy. Less than 20% of the power produced is in the form of charged particles. Also, for proposed fusion power plants, the 14.07-MeV neutrons produced need to be handled and so large mass penalties are incurred for extensive neutron shielding and dynamic energy conversion equipment.

As an alternative to DT fuel, several authors[3,4,5] have proposed using deuterium (D) and the light isotope of helium (^{3}He) as the fusion fuel (D^{3}He) for space propulsion. Although D^{3}He requires a higher temperature and longer confinement time to ignite than DT, most of the energy produced is in the form of charged particle kinetic energy. It appears feasible to

ignite D^3He in near-term DT fusion reactors[6,7]. The D^3He reaction is written as (energy in MeV):

$$ {}^{2}_{1}D_{(0.09)} + {}^{3}_{2}He_{(0.09)} \rightarrow {}^{1}_{1}p_{(14.7+0.144)} + {}^{4}_{2}He_{(3.7+0.036)} \; . $$

Neutrons are not produced in the D^3He reaction itself, but are produced in relatively few side reactions such as the deuterium with deuterium reaction (DD). These reactions will be defined later. In the D^3He reaction itself all particles produced are charged particles.

Recommended Reactor and Fuel

Therefore, we propose that the open MCF configuration, employing D^3He fuel is the preferred application of fusion technology to space propulsion.

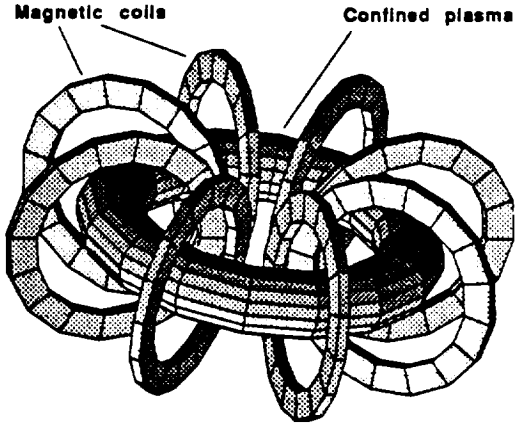

Figure 1. "Closed" magnetic-confinement example.

Another consideration is total system mass. The ICF and closed-field MCF have all been proposed for use as space fusion propulsion systems[8,9], with extremely large system masses (ranging from 1,200 to 6,000 metric tons) being typical. This is due to massive active cooling systems, and the dynamic conversion equipment to convert the fusion energy into useful thrust. The MFPS proposed here reduces system mass to 460 metric tons.

The Magnetic Mirror

The Mirror Fusion Propulsion System (MFPS) is the result of an evolutionary path of experiments and studies of the Magnetic Mirror. We briefly describe magnetic mirroring mechanics and its evolutionary path.

Basic Mechanics. The principle of magnetic mirroring involves the motion of charged particles (ions and electrons) along magnetic field lines. As the magnetic field strength increases, i.e. as the magnetic field lines converge, the charged particles are forced to reverse direction. An example of magnetic mirroring occuring in nature is Earth's magnetic field trapping and accumulating charged particles to form the Van Allen radiation belts[10]. In this case, the converging field lines occur near the Earth's north and south pole.

Plasma containment can be understood from the relation that describes the repelling force experienced by a gyrating particle in a magnetic field gradient:

$$ F = \mu(-\nabla B) \qquad (1) $$

where $\mu = \left(\frac{mv_\perp^2}{2} \cdot \frac{1}{B} \right)$ is the magnetic moment, ∇B is the magnetic field gradient, B is the strength of the magnetic field, m is the ion or electron mass, and $v_\perp$ is the charged particle velocity perpendicular to **B**.

For a particle to feel a repelling force it must have a velocity component perpendicular to the magnetic field vector. Consequently, particles with nearly all of their velocity parallel to the magnetic field will probably escape the magnetic bottle.

Simple Mirror. Experiments with magnetic mirrors for the purpose of containing a plasma began in the early 1950s[11,12,13] and were called 'Simple' Mirrors. A simple mirror experimental setup is shown schematically in Figure 2a. The two large coils (one on each end) produce stronger magnetic fields at the ends relative to the center to produce the increased magnetic field gradient (see Figure 2b). The slow plasma leakage rate verified that the stronger magnetic fields at both ends of the solenoid tend to reflect plasma. Unfortunately, a large "+" potential develops which enhances plasma leakage.

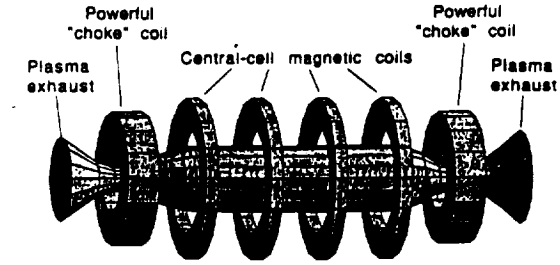

(a) A simple mirror magnet assembly.

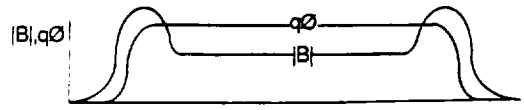

(b) All magnet coils = ON.

Figure 2. A simple mirror setup showing (a) the magnet assembly and (b) the magnetic and potential field profiles with all magnets energized.

Tandem Mirror (TM). The TM was invented independently by Dimov, et. al.[14], and by Fowler and Logan[15] to overcome the plasma leakage problem.

The basic idea behind the TM is to place two smaller mirror 'cells', or plugs, at either end of the central,

'simple' mirror cell, resulting in a string of cells or a 'tandem' mirror. Plasma is introduced into all three mirror cells with the highest plasma density maintained in the plug mirror cells[16]. Very large electrostatic potentials are formed in these plug cells. The TM reduces plasma leakage through the end plug cells because the central cell ions are bounded by the two large electrostatic potentials on either end. Any plasma ion from the central cell that climbs the magnetic gradient also approaches the large positive and repelling electrostatic potential of the plug mirror cell. Unfortunately, the two end mirror cells (plug cells) experience exorbitant electron and ion loss rates in addition to high Bremsstrahlung (x-ray) losses due to their elevated temperature relative to the central cell electrons[17].

Thermal Barrier Tandem Mirror (TBTM). To increase Q further over that of the TM, Baldwin and Logan[18] proposed the "thermal barrier" concept in 1979. This is a method to "thermally isolate" the hot plug electrons from the relatively cool central cell electrons. This allowed the plasma density in the plugs to drop below that in the central cell, and yet still maintain the high "+" potential peaks in these regions required for electrostatic mirroring. The result is a much reduced external heating requirement for the plug electrons. The Tandem Mirror Experiment Upgrade[19] (TMX-U) experiment at LLNL validated the thermal barrier concept, showing a factor of nine decrease in the central cell loss rate over the conventional TM.

Mirror Evolution

Figure 3 is a comparison of the success in improving axial plasma confinement for the simple mirror, the conventional tandem mirror, and the thermal barrier tandem mirror (TBTM). The low ion density regions (Figure 3c) have allowed the TBTM to achieve the desired high central-cell ion density.

Design Studies

MARS. The Mirror Advanced Reactor Study[20] (MARS), completed in 1984, combines a well-characterized method of MHD stabilization, with a more effective axial containment scheme over the TBTM. The plug coils for MARS are shown in Figure 4a. However, the end plug schemes had become very complex.

MINIMARS. A new commercial reactor design study based on a simplified plugging scheme[21] was completed in 1986 and was called MINI-Mirror Advanced Reactor Study[22] (MINIMARS), and is shown in Figure 4b. The resulting short, compact end cells enable ignition to be achieved with much shorter central-cell lengths which considerably improves the economy of scale characteristics for small (250-600 MWe) reactors.

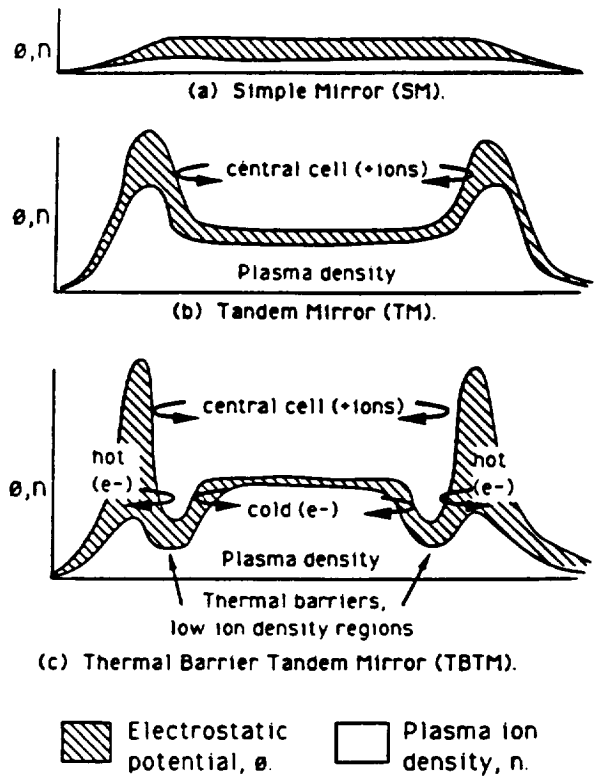

Figure 3. Comparison of electrostatic potential and plasma ion density: (a) Simple Mirror, (b) TM, and (c) TBTM.

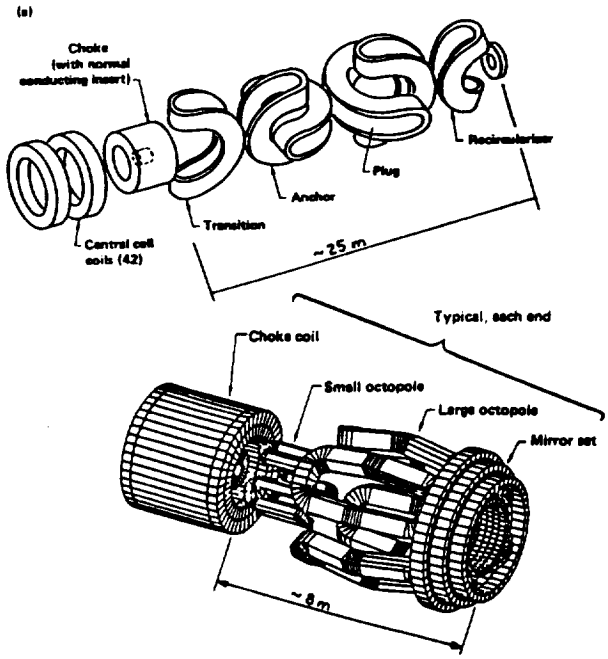

Figure 4. End-plug schemes: (a) for the Mirror Advanced Reactor Study[20] (MARS); and (b) a simpler end plug for MINIMARS[22].

Part 2
Design Principles for Space Fusion Propulsion

We next describe and show by example the importance of three design principles that are applied to the MINIMARS reactor design to create a space propulsion system with minimal power plant mass while maintaining maximum specific power (kw/kg) for thrust:

1) optimize the "fuel-mix" and plasma temperature to minimize waste radiation,
2) provide direct access to space for waste radiation,
3) operate components as blackbody radiators.

Principle #1: Optimize the "fuel-mix" to Minimize Waste Radiation

The D^3He plasma mix and plasma temperature must be optimized for highest system efficiency and power available for thrust. This will maximize system performance, and minimize the shielding mass and cooling system mass necessary to dissipate the waste heat accumulated in system components.

Fuel-Mix. There are four primary types of radiation produced from the D^3He reaction, resulting in 'waste energy'. The fuel mix and plasma temperature of the D^3He must be optimized to minimize the total waste energy. Fuel mix is defined as the ratio between the numbers of ions of each fuel constituent in the plasma. The radiations produced are listed here and will be discussed in greater detail later:

- Bremsstrahlung (x-ray),
- synchrotron (microwave),
- neutrons, and
- plasma transport (heating).

Figure 5 is a representative case of the importance of "fuel-mix" in regard to each of the four plasma radiation terms and how they relate to the percent of total fusion power that is available for thrust at 90 keV. Many authors have mistakenly given neutron energy all of the emphasis while ignoring the other radiations produced such as the Bremsstrahlung. Figure 5 demonstrates that to save a mere 1.4 % in neutron power - moving from a fuel-mix of unity to 2.4 - you must pay a 25 % penalty in Bremsstrahlung (x-rays) and, to a lesser extent, a penalty in synchrotron radiation as well. The minimum of the sum of the four plasma radiation terms occurs with a plasma ^3He-to-D "fuel-mix" of 0.5, or about one ^3He ion for two D ions.

Plasma Temperature. The net percent power available for thrust is shown in Figure 6 for temperatures below and above the optimum computed temperature of 90 keV. All four of the plasma-power loss terms are included; neutron, Bremsstrahlung, synchrotron, and plasma transport. This figure illustrates that the thermodynamic optimal operating point is about 90 keV. Thus, we propose a ^3He-to-D "fuel-mix" of about 0.5 at a plasma temperature of 90 keV which results in 64 % of the total fusion power remaining available for thrust (P_{AFT}) (see Figure 5). The power available for thrust represents the fusion energy remaining as charged-particle kinetic energy, which is used to heat the propellant.

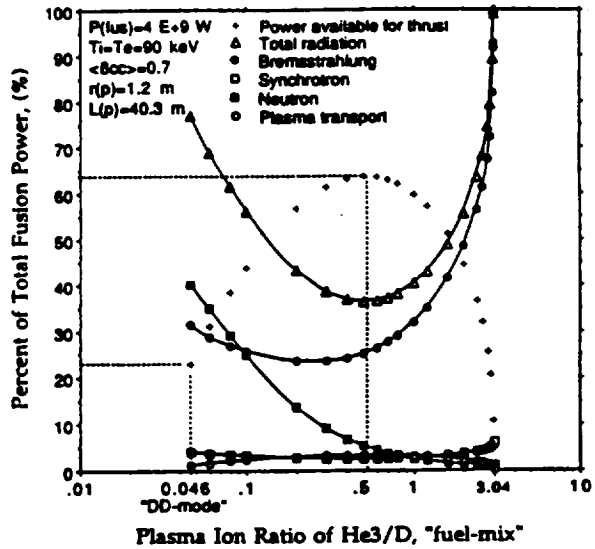

Figure 5. Radiation power losses versus "fuel-mix."

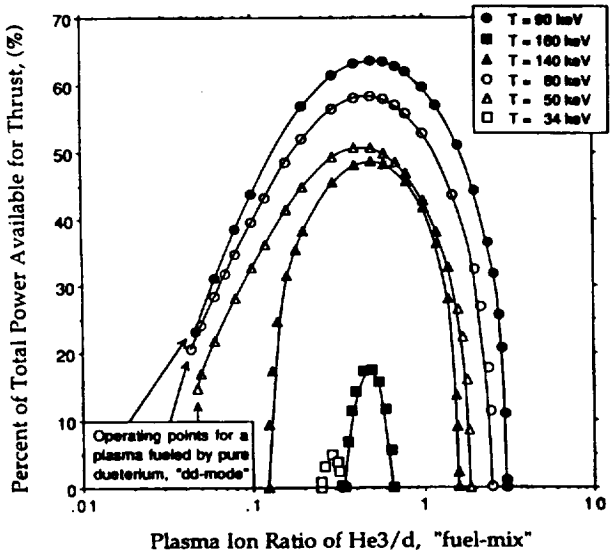

Figure 6. Percent power available for thrust versus "fuel-mix" @ 34, 50, 60, 90, 140, and 160 keV.

Primary and Secondary reactions. To accurately model the energy and radiation produced, tracking the relevant fusion side reactions was necessary. For a plasma fueled by pure D and ^3He, we tracked the reactions listed in Table 1. Fusion products are also fusionable; e.g., the two DD reactions [2] & [3] of Table 1 produce tritium and helium-3. These products

in turn act as fuels themselves as in reactions [5] through [10] of Table 1.

Table 1. D^3He fusion reactions[23,24]. (energy in keV)

Fuel-Fuel (FF) fusion reactions		
D^3He	----> P (14681) + ^4He (3670)	[1]
DD	----> P (3024) + T (1008)	[2]
DD	----> N (2450) + ^3He (817)	[3]
$^3He^3He$	----> P (5716)+ P (5716) + ^4He (1429)	[4]
Fuel-Product (FP) fusion reactions		
DT	----> N (14069) + ^4He (3517)	[5]
T^3He	----> D (9546) + ^4He (4773)	[6]
T^3He	----> N (5374) + P (5374) + ^4He (1344)	[7]
T^3He	----> P (10077) + N (1612) + ^4He (2015)	[8]
Product-Product (PP) fusion reactions		
TT	----> N (5034) + N (5034) + ^4He (1259)	[9]
PT	----> N (-573) + ^3He (-191)	[10]

"Shelling" the fuel pellet. It is desirable to use fuel-pellet injectors to feed fuel to the plasma. The compactness and short lengths for pellet acceleration make the electromagnetic fuel-pellet injector a minimal mass subsystem for plasma feeding, and thus a subsystem of choice. However, short acceleration lengths translate into large stresses on the fuel pellet. A DD-ice shell is incapable of meeting the stress requirements[25]. Consequently, small amounts of a light metal (such as lithium-6 or -7, or beryllium-9) may be added to the "ideal" fuel, D^3He, to form a strong fuel pellet shell.

Elements with Z>2, and therefore more electrons, cause a degradation to the power available for thrust by producing more Bremsstrahlung radiation. In our analysis, we followed the reactions added by the addition of these light metal ions. As an example, the four reactions added to the plasma reactions from the use of Lithium-7 are listed in Table 2. We propose encapsulating ^3He and D in a lithium deuteride (LiD) shell or beryllium shell for which we limit the Li or Be to a small atom percent (< 6 %) of the overall fuel pellet content. The reduction in power available for thrust is about 6%.

Table 2. D^3He^7Li fusion reactions[23].

Fuel-Fuel (FF) reactions, [1] - [4] and:		
D^7Li	---> N (10082) + ^4He+^4He (2x2521)	[19]
$^3He^7Li$	---> N+P (2x3852) + ^4He+^4He (2x1512)	[20]
Fuel-Product (FP) reactions, [5] - [8] and:		
P^7Li	---> ^4He (8674) + ^4He (8674)	[23]
T^7Li	---> N+N (2x6049) + ^4He+^4He (2x1512)	[24]
Product-Product (PP) reactions: [9] and [10].		

Radiation Types Produced. The fusion process produces either charged ions or neutrons. Neutrons immediately leave the plasma due to their being unaffected by the magnetic field, and may interact with engine components in their path. The charged particles lose some of their power to the radiation produced: Bremsstrahlung, synchrotron radiation, and plasma transport. The power that remains available for thrust is:

$$P_{AFT} = P_{FUS} - P_{Brem} - P_{syn} - P_{\chi} - P_n \qquad (2)$$

where P_{AFT}, is power available for thrust, P_{FUS} is total fusion energy produced, P_{Brem} is Bremsstrahlung produced, P_{syn} is synchrotron radiation not reflected back to the plasma, P_C is plasma transport, and P_n is neutron power. To achieve the largest power available for thrust, P_{AFT}, we must minimize the sum of the four power-loss terms: P_{Brem}, P_{syn}, P_C and P_n.

Bremsstrahlung Radiation. Bremstrahllung radiation is produced when any charged particle undergoes an acceleration due to the attraction or repulsion of an electric field. Bremsstrahlung emitted from a plasma has a continuous spectrum ranging in frequency from hard x-rays to soft x-rays. The equations used to determine the Bremsstrahlung power losses are summarized by McNally[26].

Bremsstrahlung produced is proportional to plasma electron density, the effective charge seen by the plasma electrons, and the electron temperature. We try to minimize each of these parameters in order to maximize power available for thrust. To minimize the electron density and ion atomic charge, we optimize the "fuel-mix," and use pellet shells with low atomic number. To minimize the temperature, we use fuels with large fusion-reaction cross-section at low/medium temperatures (<160 keV).

Synchrotron Radiation. Synchrotron radiation is produced when a charged particle undergoes acceleration due to its motion around its gyro-center, or magnetic field line. Out of the four types of radiation produced, it is the synchrotron radiation which can be reflected back into the plasma. It is relatively easy to reflect a major portion of the synchrotron (microwave spectrum) back into the plasma by use of a reflective shell. The reflected synchrotron is readily absorbed by the plasma. Without a synchrotron reflector, an appreciable fraction[27] of the plasma power is lost, thereby reducing the power available for thrust.

Plasma transport. MFPS requires radial plasma transport in order to produce its "scrap-off" halo plasma that mixes with propellant ions before being directed to the exhaust nozzle. There are a variety of theoretical predictions for transport coefficients for mirror plasmas. Rather than attempt theoretical calculations (based on many intangibles), our model simply and conservatively assumes that 5% of the charged particle power remaining after Bremstrahllung and synchrotron radiations are removed, radially diffuses through the plasma halo to the inside wall of

the synchrotron reflector prior to exiting the exhaust nozzle.

Neutrons. For the D^3He-fueled plasma, neutrons are produced in reactions [3], [5], and [7]-[10] of Table 1. The DT reactions produce the most neutron power; however, the DD reactions produce a higher neutron flux.

Principle #2: Providing Direct Access to Space for Waste Heat

We find that the primary system performance limiter is the waste heat absorbed by the engine, with Bremsstrahlung being predominant. Between 35 and 50 % of the total fusion power will be waste heat. Minimizing the heat absorbed by the engine components will allow higher total fusion power, minimized engine component temperatures, and minimized mass for cooling systems. To minimize the percentage of waste heat absorbed by the engine, we provide the waste heat with as much direct access to space as possible. The methods to allow this direct access to space from the engine are discussed in Part 3.

Principle #3: Operate Components as Blackbody Radiators

All space fusion propulsion systems will absorb some waste heat for which there are two general methods of heat removal: (1) operate as many components as possible in a passive cooling mode or (2) provide active cooling. The Mirror Fusion Propulsion System (MFPS) operates its major components as passive "blackbody" radiators as a means to reduce active cooling system mass.

Part 3
Mirror Fusion Propulsion System (MFPS) Design Overview

Our nominal MFPS is a 460,000 kg mirror fusion propulsion/power plant that produces continuous thrust. Nominally, the MFPS produces 4 GW of fusion power, with a net exhaust-jet power of about 2 GW and therefore a specific power of about 4.3 kW/kg. About 31 grams per second of hydrogen propellant is injected into the 2-GW plasma halo to achieve a nominal continuous thrust of 11,000 N. This results in total vehicle accelerations of 1-to-1.5 cm/sec^2 at a maximum specific impulse of 37,000 seconds.

MFPS is designed for a nominal lifetime of 6 to 8 piloted Mars-type missions. It can be constructed in orbit, from three segments weighing 150,000-to-160,000 kg each (based on the Synthesis Report's Heavy-Lift Launch Vehicle recommendation[1]).

MFPS Configuration and Major Components

The major subsystems and components of the MFPS are configured along and roughly axisymmetric to a longitudinal axis that goes through the center of the fusion plasma. The entire MFPS is about 79 m long and 8 m in diameter over most of its length. MFPS has eight major components or subsystems as illustrated in Figure 7. The estimated masses of the major MFPS components are shown in Table 3. The following sections discuss the major MFPS components.

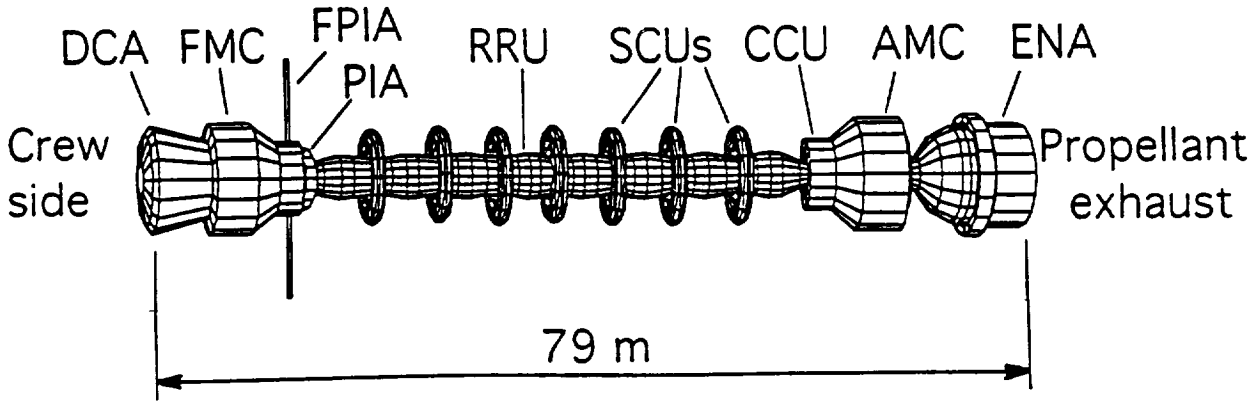

ATCS	Active Thermal Control Subsystem (not shown)	RRU	Reflector-Radiator Unit
DCA	Direct Converter Assembly	SCU	Shield-Coil Unit
FMC	Forward Mirror Cell	CCU	Choke Coil Unit
CMC	Central Mirror Cell	AMC	Aft Mirror Cell
FPIA	Fuel Pellet Injection Assembly	ENA	Exhaust Neutralizer Assembly
PIA	Propellant Injection Assembly	HCS	High-Compression Structure (not shown)

Figure 7. The Mirror Fusion Propulsion System (MFPS) - drawn to scale.

Table 3. MFPS major component masses.

Component	Metric Tons
CMC	
RRU	14 (b)
SCUs	168 (a)
CCUs	42 (b)
FPIA	8 (c)
Structure (HCS)	104 (b)
AMC/FMC	48 (c)
PDS	6 (b)
PCS	14 (b)
ENA	6 (c)
DCA	5 (c)
ATCS	45 (b)
Total	460

(a) optimized (b) estimated (c) by assignment

Central Mirror Cell (CMC) Subsystem Descriptions and Design Drivers

The function of the CMC is to contain the fusion core plasma in a stable, ignited mode. The CMC consists of six components or subassemblies: (1) the Reflector-Radiator Unit (RRU), (2) seven Shield-Coil Units (SCUs), (3) two Choke Coil Units (CCUs), (4) a Fuel Pellet Injection Assembly (FPIA), (5) a Propellant Injection Assembly (PIA), and (6) a High-Compression Structure (HCS).

Reflector-Radiator Unit (RRU). The RRU is a thin-walled rippled tube that surrounds the plasma. The RRU wall is composed of three layers: (1) the inner layer is a thin foil of molybdenum 10-50 mm thick, (2) the middle layer is graphite, about 1 cm thick, and (3) the third layer is carbon fiber, also about 1 cm thick. The RRU's layers perform four functions: (1) the molybdenum layer reflects synchrotron radiation back into the plasma where it is absorbed, thereby increasing the power available for thrust; (2) the graphite layer aids stabilization of the plasma by acting as an electrically conducting wall, producing an image-current counter force to growing plasma instabilities; (3) the carbon fiber layer acts as a "blackbody" radiator, thereby minimizing external cooling-system mass, and provides directional structural strength; and (4) the three layers together allow most of the neutrons and over half of the plasma x-rays (Bremsstrahlung) to pass directly through the RRU into space (see Figure 8), thereby reducing the RRU temperature.

The RRU also absorbs the plasma transport heat, synchrotron radiation, and re-radiated heat from the Shield-Coil Units (SCUs). The outer carbon fiber surface then acts as a "blackbody" radiator, with most of the radiated heat going directly into space. The RRU surface temperature may be determined from the Stefan-Boltzmann blackbody radiator law. The minimum computed temperature for the optimized RRU is 2200°C, and is reached with our proposed spacing of SCUs (from Design Principle #2) and D^3He fuel mix ratio of 0.5 (from Design Principle #1). The heat flow is illustrated in Figure 8. We would like to place the SCUs as wide apart as possible, but plasma stability requirements place a maximum limit on the spacing.

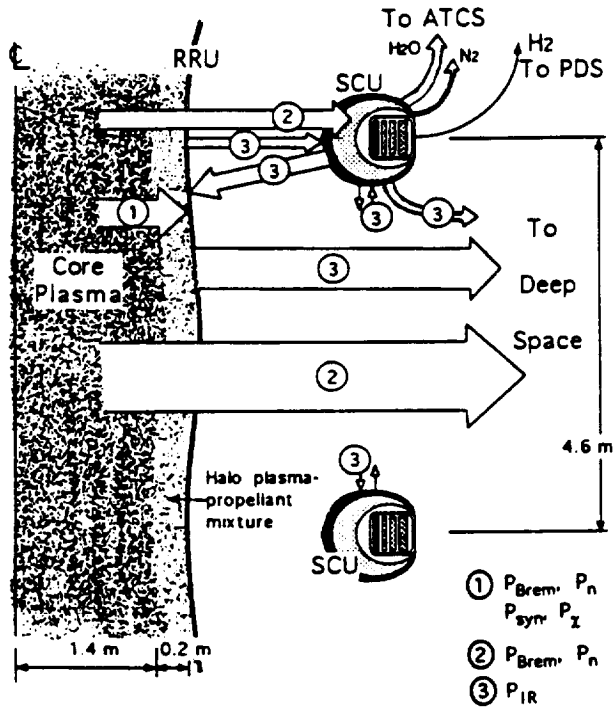

Figure 8. Waste power flow in MFPS.

Shield-Coil Units (SCUs). The nominal MFPS has seven central cell coils, and two choke coils, one on each end of the central cell. The mirror ratio is 5; i.e., the magnetic field at the choke coil is 5 times that at the center of the CMC. The SCU shields protect the superconductor by absorbing or scattering radiation.

The radial pressure of the reacting D^3He and other fusion reactions in the 40-meter-long CMC is contained by the magnetic field produced by the seven SCUs (producing 6.6 Tesla vacuum field each). The axial plasma pressure is contained mainly by the high-field (33 T vacuum) choke coils at each end. The SCUs are placed along the length of the central cell, forming a maximum magnetic field ripple of 15 % as seen in Figure 9. Spacing between SCUs is key in setting the magnetic 'field ripple'. The overriding factor influencing the magnetic ripple between two current rings (coils) is the ratio of the separation distance between coils to the radius of the coils. Magnetic field ripple is defined as:

$$B_{(ripple)} = \frac{B_{MAX} - B_{MIN}}{B_{AVE}} = 2 \cdot \frac{B_{MAX} - B_{MIN}}{B_{MAX} + B_{MIN}} \qquad (3)$$

The ripple field aids stabilization of the central cell plasma[28,29], reduces end-plug technology requirements, and improves the plasma power density.

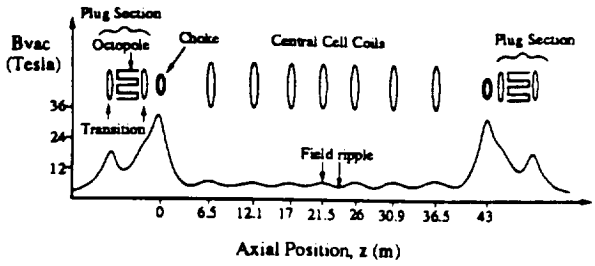

Figure 9. Magnetic field ripple.

Superconductor Winding Pack. In our winding pack characterization we found that the significant factor in determining the mass of an individual SCU (and half of the mass of the entire MFPS) hinges on the volume of the superconductor winding pack. We desire to minimize the volume of the winding pack to limit the volume and masses of the concentric shields. This situation is illustrated in Figure 10. To minimize the winding pack volume and cross-section, we propose using bismuth (Bi)- or thallium (Tl)-based superconductor. The literature[30,31,32,33] gives us confidence that these new superconducting materials can be brought to maturity in the near-term. For our nominal MFPS, we desire a superconductor that can meet the design criteria that we call the "Three 30s": 30 kA/cm^2 at 30 K and 30 Tesla. We based these criteria on achievements made[34] in the field and on theoretical estimates[32] that exceed these MFPS criteria.

Current winding pack design practice includes four parallel superconducting circuits, one of which is redundant, and safety features that monitor and respond to the superconductor 'going normal'. The "hoop" stresses generated by the magnetic field are handled internal to the winding pack and for each circuit individually.

Superconductor shielding. Shielding is required to protect the central cell superconducting magnets from x-ray, neutron and neutron capture-gamma radiation. The shielding requirement is set by the radiation limits for the superconductor and insulator. Neutron irradiation to "normal superconductors," e.g., NbTi, degrades the critical current density. It appears that the desired thallium and bismuth-based high-Tc superconductors, and others, are more resistant to neutron irradiation[33]. We define the total desirable fast (>0.1 MeV) neutron fluence limit as 3 x 10^{22} n/m^2. With this criterion in mind, we found that the greatest concern is removal of heat deposited in the superconductor. We use our propellant (liquid hydrogen) as the superconductor coolant, and it is the coolant/propellant mass flow at full engine power that sets the limit on the amount of heat allowed to deposit in the winding pack. The coolant/propellant is circulated in the coil until it reaches the coil's operating temperature limit, and then it is delivered to the Propellant Injection Assembly (PIA).

Shielding Design Problems. The SCU receives heat from three sources: (1) the plasma Bremsstrahlung and neutrons, both of which penetrate the RRU wall, (2) neutron capture gamma, and (3) thermal radiation from the RRU wall and the adjacent SCUs. Given the x-ray and neutron radiation with differing penetrating, absorption, and scattering properties, we identified five design problems that must be solved simultaneously to achieve a minimum-mass shield while maximizing performance:

1. Catch as much of the penetrating radiation near the outer surface of the outermost shield as possible so that the heat-conduction path to the outer blackbody surface is minimal.
2. Reduce the deeply penetrating 2.45 and 14.07 MeV neutrons to a level survivable by the superconducting material for a number of manned Mars-type missions.
3. Reduce the neutron capture gamma to a level also surviveable by the superconductor.
4. For heat not removed by passive means, provide a means of heat removal and transport for external heat rejection.
5. Minimize the heat deposited in the winding pack to minimize the propellant needed for cooling in order to maintain a high engine specific impulse.

Superconducting Shield Design Solutions. The SCU shield cross-section is shown in Figure 10. The SCU shield component mass breakdown is shown in Table 4. The solution to shield design problem #1 is to use a high-emissivity, high-temperature material with excellent neutron- and x-ray-stopping characteristics. For our nominal total engine power of 4 GW, the solution is an outer x-ray-absorbing tungsten or tantalum shield, that for each SCU intercepts and disperses a total of 26.6 MW (14.1 MW x-ray, 11.9 MW infrared, and 0.6 MW neutrons). The neutron-absorbing carbon-carbon shield absorbs and disperses 2.75 MW (2.5 MW neutrons and 250 kW x-ray). The two outer shields (tungsten and carbon-carbon) are thermally separated from the remainder of the SCU by insulation such as pyrolized carbon aerogel[35]. The SCU outer surface temperature is estimated at 2000°C at full power. Unfortunately, the only excellent x-ray stoppers that can stand the high temperatures - tungsten and tantalum - also have high densities.

A solution to shield design problem #2 is to place enough neutron shielding material between the plasma and the superconductor to catch most of the x-ray and

Table 4. SCU Component Masses.

Component	Mass (kg)
outer tungsten shield	1,900
carbon-carbon shield	3,950
lithium hydride shield	3,650
inner shields	1,100
winding pack	13,200
thermal insulation	200
Total	24,000

neutrons that penetrate through the outer shield. However, we desire to do this with the least amount of mass possible. The next shield in toward the winding pack, is made of lithium hydride and contains the bulk of the SCU volume. Fortunately, lithium hydride has a specific gravity of only 0.82 g/cm^3 and is a good neutron stopper. The lithium hydride shield absorbs nearly all of the x-ray and neutron radiation not absorbed by the outer shields which totals 650 kW (585 kW neutrons, 30 kW x-ray, and 35 kW thermal from the insulation). The energy absorbed here is rejected to an active thermal control subsystem.

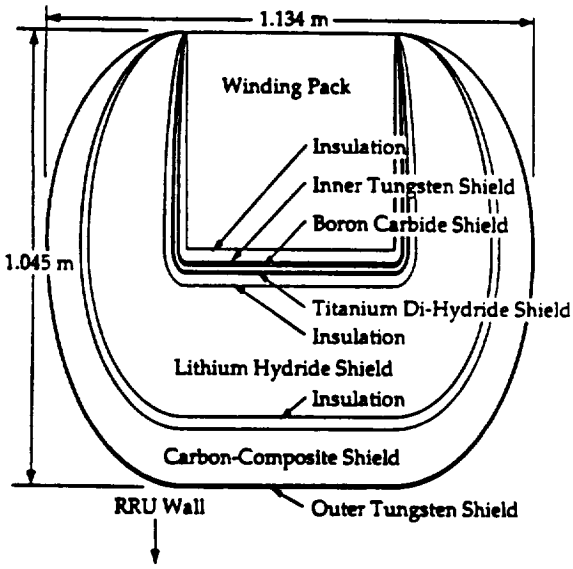

Figure 10. Optimized Shield-Coil Unit (SCU), (drawn to scale).

The three inner shields, titanium di-hydride, boron carbide, and tungsten (capture-gamma stopper), make up the final shielding needed to reduce the winding pack heat load and are thermally insulted from the lithium hydride shield and from the winding pack by an aerogel[35]. These shields further reduce the x-rays and neutrons reaching the winding pack, while providing the solution to shield design problem #3 - the need to stop the capture-gamma. These three inner shields absorb 4.8 kW of energy (1 kW from the insulation, 2.2 kW x-ray, and 1.6 kW neutrons) and reject their heat to the active thermal control subsystem.

A solution to shield design problem #4 is to provide a water-cooling system for the middle shield and a nitrogen-cooling system for the shields nearest the winding pack.

The winding pack, described in an earlier section, absorbs about 2.4 kW of the remaining x-rays, neutrons, and the heat flowing through the insulation. In minimizing the heat deposited to in the winding pack (shield design problem #5), the hydrogen propellant required to acquire this heat in an open heat cycle is only 30 grams/second, at an average temperature of 20-25 K. Overall specific impulse of the MFPS is maintained at 37,000 seconds.

The Fuel Pellet Injection Assembly (FPIA). The FPIA chosen for MFPS uses mechanical (centrifugal) and electromagnetic-railgun technology for fueling the core plasma. The FPIA is a two-stage system consisting of a centrifugal particle injector to reduce pellet erosion in the low-speed portion of the railgun that boosts the pellet speed to between 10 to 30 km/s. The railgun technology is relatively well characterized[36,37], efficient, and compact. For optimum pellet penetration, injection occurs near the forward Choke-Coil Unit (CCU) where the plasma radius is at a minimum, lessening the pellet velocity requirement.

Choke-Coil Units (CCUs). The two choke-coil units are powerful magnetic coils, with one placed at each end of the Central Mirror Cell (CMC) to provide a steep magnetic gradient that mirrors most of the plasma back to the cell's center (~ 90%). The other 10% scatters into the "loss cone" only to be reflected back by the positive plug potential (electrostatic mirroring), returning to the central cell. The nominal case mirror ratio is five; i.e., the vacuum magnetic field at the choke-coil position is five times larger than at the center of the central cell, resulting in a centerline vacuum magnetic field of 33 Tesla at the choke coil positions.

The High-Compression Structure (HCS). The HCS is the primary load-carrying structure of the MFPS that holds the coils in place within the three mirror cells. The HCS has a dual role: (1) to provide the structural means to prevent the SCUs, CCUs, and the octopoles from coming together due to their mutually attracting magnetic forces, and (2) to shield the fluid and utility lines routed to each SCU and CCU.

The HCS consists primarily of eight-to-sixteen "columns" of varying thickness over the length of the three mirror cells. These columns can be made of such high-strength, high-temperature materials as titanium boride, laminated with high temperature, high-compression carbon aerogel[35]. The loads that the

structure must carry are nearly entirely magnetic in origin, and so the vehicle flight accelerations which are smaller by four orders of magnitude can be ignored. Peak compressive loads occur at the center central-cell magnets during nominal full-power operation.

Forward and Aft Mirror Cells (FMC and AMC)

The FMC and AMC, located forward (crew side) and aft (propellant-exhaust side) of the CMC, respectively (see Figure 7), each consist of one large octopole magnet and several shaping magnets that aid central cell plasma stability during startup and axial plasma confinement during all operations. The FMC is borrowed from the MINIMARS[22] design study.

The AMC is configured similarly to the FMC. The exceptions are that the choke coil magnetic field and electrostatic potential are reduced relative to the FMC in order to provide the axial asymmetry required to allow ~ 94% of the power available for thrust to exit into the Exhaust Neutralizer Assembly (ENA). The remaining 6% is directed to the Direct Converter Assembly (DCA) for conversion to electrical power.

Direct Converter Assembly (DCA)

The DCA, located forward of the FMC, directly converts escaping charged-particle kinetic energy to electricity. The electrical power is used for space vehicle electrical loads and recirculation power for fusion reactor systems. The gridless direct converter is adapted from MINIMARS[22]. It is extremely lightweight due to its small external structure requirement.

Reactor Ignition Subsystem.

We propose to ignite the MFPS using the DT reaction because of the relatively low ignition temperature (10 keV) and minimized external-energy investment needed. The energy needed - between 5 and 6 GJ - will be dumped into the heating and magnet systems over the 20-to-90-second period required to ignite the DT plasma. Once ignited, the reactor is quickly brought to self-sustaining, with the direct converter producing electrical power from the escaping central-cell ions. This power is transferred to the superconducting magnetic containment coils to further increase the magnetic fields, which are subsequently raised to their normal operating fields. Meanwhile, D^3He fuel pellets have replaced the DT pellets. MFPS is now operating at 4 GW thermal fusion power with 39 GJ stored in its magnetic fields.

Post[38] has developed an advanced carbon-fiber composite-flywheel energy-storage system ideally suited to MFPS ignition requirements. These flywheel units pack about 200 whr/kg with all supporting structural weight and lifetime factors included. To minimize cable mass, the 90 flywheel units operate at the location where the energy is needed. Total ignition energy source mass is 12,500 kg. There are nine flywheel units located at each SCU and another 24 for both the aft and forward mirror cells (electrostatic plugs), their heating systems, and the choke coils.

Propellant Delivery Subsystem (PDS).

The PDS is responsible for pumping the liquid-hydrogen propellant through the superconducting coils to provide cooling of the coils and then injecting the heated propellant into the CMC.

Liquid hydrogen propellant, stored at ~15 K, enters the winding pack and removes heat primarily through nucleate boiling. Its temperature upon exit of the winding pack is about 25 K, vapor form. Under these conditions, 1 gram/sec of H_2 (liquid) at 16 K, heated to 1 gram/sec of H_2 (vapor) at 25 K and modest pressure, will remove about 800 watts of heat. It is the propellant flow rate that determines the allowable power deposited in the winding pack.

The 25 K hydrogen propellant is then directed to high temperature areas for preheating before injection into the plasma halo near the Forward Mirror Cell on the central-cell side of the choke coil. There, the propellant is mixed, heated, ionized, and then exits into the Exhaust Neutralizer Assembly (ENA) with about 50 to 1000 eV/ion.

Exhaust Neutralizer Assembly (ENA)

The ENA neutralizes the plasma/propellant mixture, thereby detaching the particles from the magnetic field lines to produce thrust. The ENA contains neutral gas-injection jets for charge exchange with the hot plasma/propellant exhaust. Fowler[39] has described an exhaust neutralizer with a neutralizing efficiency[40] of ~90% and negligible loss of cold neutral gas. In the exhaust annulus, the cold gas charge-exchanges with the exhausting plasma-propellant (expellant), neutralizing the expellant. The cold charge-exchange ions make contact with the neutralizer walls, collect an electron to become neutral, and drift back into the plasma-propellant to perform another charge-exchange.

Active Thermal Control Subsystem (ATCS)

The ATCS consists of radiator panels and pump assemblies forward of the direct converter, and pipes distributing the cooling fluids to all SCUs and CCUs throughout the MFPS. The ATCS functions to remove heat from the shield layers lying between the outer shields and the winding packs of the SCUs and CCUs, and for other components requiring external cooling.

The ATCS has two subsystems. The first subsystem is a pressurized, two-phased H_2O closed-loop system removing a total of 7.4 MW from the lithium-hydride shields that protect all of the superconducting coils. This heat is rejected by radiator panels of undetermined location, but requiring about 700 m^2 area. The water temperature ranges between 545 K and 588 K.

The second part of the ATCS is a closed-loop N_2-refrigeration cycle using high-pressure, two-phase

nitrogen as a coolant. This refrigeration cycle removes about 60 kW from the inner shields protecting all of the superconducting coils. This 60 kW is pumped from 100 K to 545 K and deposited in the H_2O closed-loop system. We estimate the H_2O closed-loop system mass at 38,000 kg and that of the N_2-refrigeration system at 7,000 kg. The mass estimate includes radiators, dual-redundant piping, pumps, and fluids[41].

Part 4
Performance Comparison of MFPS With Alternate Propulsion Systems

Propulsion Systems to be Compared

We will now compare some key performance parameters of the MFPS with alternate propulsion systems - both demonstrated and envisioned. These propulsion systems are:

1) Chemical (cryogenic),
2) Nuclear Thermal Rocket (NTR) solid core,
3) NTR gas core, and
4) Nuclear Electric Propulsion (NEP) at varying power levels.

Common Vehicle Configuration. All propulsion systems were integrated into a generic vehicle configuration using common masses and common methods for the configuration. Table 5 shows vehicle components common for all propulsion systems. All five systems were required to deliver a 150 metric ton payload (landers and crew module) to Mars, and return the 50-metric ton crew module payload to Earth.

Table 5. Common Vehicle Components

VEHICLE COMPONENT	MASS (metric tons)
Payload (Landers)	100,000
Payload (Crew Module)	50,000
Structure & Avionics	30,000
Propellant	variable per mission
Propellant Tanks	10% of Propellant mass
Engine(s)	variable per system

In computing the required IMLEO for each system on each mission, iterative computations were used, with the propellant being the independent variable. Tank mass was dependent on propellant mass. No mass was set aside for residual, unuseable propellant.

Vehicle structure, communications, attitude control, power systems, thermal control, and other avionics were all packaged into a 30-metric ton mass.

Chemical System and Mission Profile. The Chemical system uses liquid oxygen and hydrogen, and is assumed to have a specific impulse of 475 seconds. This technology is used exclusively today for launch vehicles and upper stages. Specific impulse, I_{sp}, is defined as follows:

$$I_{sp} = T/(\dot{m}g) \qquad (4)$$

where T is engine thrust, $\dot{m}$ is propellant mass flow, and g is the gravitational acceleration at earth's surface. The Chemical vehicle is 'staged', i.e. one set of engines and tanks are used for the flight to Mars, and a second set of engines and tanks are used for the flight home. Engine mass for the outbound stage was 10,000 kg, and 3,000 kg for the return stage. No aerobraking is assumed for the Chemical vehicle, i.e. the mission is all-propulsive.

NTR Solid Core. The NTR solid core system uses liquid hydrogen, and is assumed to have a specific impulse of 1,000 seconds. This system technology has been demonstrated in the NERVA program, but never put to use[1]. It is assumed to have the same configuration as the NERVA engine that uses a solid core of uranium-235 to heat the hydrogen propellant. Like the chemical system, this system is all-propulsive, and 'staged' for the outbound and return flights. Engine mass outbound is 65,000 kg, and engine mass for return is 13,000 kg.

NTR Gas Core. The NTR gas core system uses a Uranium Fluoride (UF_6) plasma to heat hydrogen propellant[42]. Engine specific impulse is assumed at 3,000 seconds. Engine mass is 90,000 kg. The engine is not staged, but is used for the entire round-trip. However, empty propellant tanks are dropped off after the outbound flight to Mars is complete.

NEP. The NEP system uses a nuclear reactor fueled with uranium-235 to generate thermal power which is then converted to electricity using dynamic energy conversion systems. The electricity is then used to power ion or magnetoplasmadynamic (MPD) thrusters. System efficiency and system specific power varies with power level. Table 6 lists the electrical power ratings used, and assumed respective masses for the NEP package: reactor, radiators, dynamic conversion equipment, and thrusters[43,44]. Thrusters were assumed to have 50% efficiency. The NEP system is used for the round-trip, with empty propellant tanks dropped when reaching Mars.

Table 6. Various NEP Power Levels and Masses.

NEP ELECTRICAL POWER (MW)	NEP MASS (kg)
20	90,000
50	120,000
100	165,000
200	200,000

MFPS. The Mirror Fusion system is described in earlier sections of this paper. The MFPS engine - with

a mass of 460,000 kg, is used for the roundtrip. Empty propellant tanks are dropped when reaching Mars.

Performance Parameters to be Compared

The performance parameters to be compared, as stated in the Introduction, are IMLEO, mission flexibility, and flight time. All five of the propulsion systems are required to deliver 150 metric tons of payload to Mars, and return 50 metric tons back to Earth. As flight times vary, so will the propellant requirements and IMLEO for each system. In addition, each of these systems on different missions will show some degree of mission flexibility, i.e. an envelope of time in which the vehicle can return to Earth. We now define the missions to be carried out by the five propulsion systems.

Two Basic Flight Strategies. These five systems employ one of two basic flight strategies characterized by differing means to achieve a transfer orbit or trajectory: 1) high impulse acceleration, and 2) low continuous acceleration.

The first strategy, high impulse acceleration, is the standard means used today, i.e. high acceleration is used at one point in a vehicle's orbit to create a ΔV to achieve a transfer orbit to Mars. The standard equations of hyperbolic planetary passage were used and applied to the Method of Patched Conics[45,46]. The ΔV required for trans-Mars injection from Earth, was the change in velocity from orbital velocity in LEO, to the velocity necessary for the proper transfer orbit to Mars, from a point in the vicinity of Earth. Upon reaching Mars, another ΔV is imparted to the vehicle necessary to achieve Low Mars Orbit (LMO). The return flight to Earth is similar in execution. Figure 11 shows the results of the computations, as flight time versus angle travelled about the Sun, Du, for curves of constant ΔV. The ΔV curves represent the ΔV's required for a one-way flight and is the sum of the ΔV to escape Earth, and the ΔV to be captured by Mars. The Chemical, NTR solid core, and NTR gas core systems employ the strategy of high impulse acceleration for flight.

The second flight strategy uses low continuous thrust to create constant accelerations on the order of 10^{-3} to 10^{-4} G, to allow the vehicle to steadily accelerate[47,48,49,50]. Although theoretical work exists in the literature, this strategy of flight has never been used for interplanetary flight. Unlike high impulse acceleration flight, where the transfer orbit is achieved in only minutes, the transfer orbit of the space vehicle is constantly changing over the entire length of the flight.

Our continuous low-acceleration trajectory is made up of three phases: escape spiral, heliocentric transfer, and capture spiral.

All three phases model the radial and tangential components of distance, velocity, and acceleration - either about a planet (escape or capture) or the Sun (heliocentric transfer). The following equations define the orbital radial and tangential component accelerations used in our analysis[47]:

$$\ddot{r} = r\dot{\theta}^2 + A\sin\phi - g \qquad (5)$$

and

$$\ddot{\theta} = \left(A\cos\phi - 2\dot{r}\dot{\theta}\right)/r \qquad (6)$$

where $r, \dot{r}, \ddot{r}$ are radial components of displacement, velocity, and acceleration, respectively; $\theta, \dot{\theta}, \ddot{\theta}$ are the inertial angle, angle rate, and angle rate change associated with the tangential components of displacement, velocity, and acceleration, respectively; ϕ is the angle between the thrust vector and the tangent to the circular orbit that intercepts the point at the vehicle location (the thrust vector is in the orbital plane); 'A' is the vehicle acceleration produced by the thrust; and g is the local gravitational acceleration.

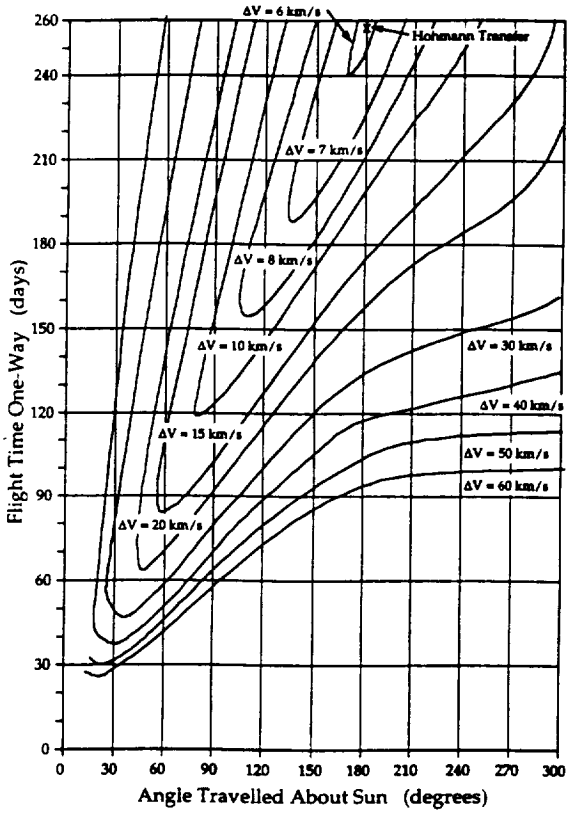

Figure 11. Flight Time vs. Δv for constant ΔV.

The flight begins with an 'escape spiral' from LEO, outward from Earth to the edge of the sphere of influence with the Sun. The flight is then computed heliocentrically, where the flight is a partial outward spiral about the Sun. The vehicle achieves its greatest velocity somewhere near the midpoint in the flight,

where the vehicle's acceleration vector is re-pointed to slow down and allow capture at Mars. The acceleration and deceleration phases are separated by a 12-hour coast period to simulate a reasonable time for the vehicle to execute an attitude change for the new acceleration vector. In the vicinity of Mars, a 'capture spiral' is then computed about Mars. Computationally, it is identical to the reverse of an escape spiral from Mars. Figure 12 shows the results of the computations, as flight time versus angle travelled about the Sun, $\Delta\upsilon$, for curves of constant acceleration. Acceleration magnitude for each flight is constant throughout the flight, from Earth escape spiral to Mars capture spiral.

The NEP and MFPS systems employ the low continuous acceleration strategy of flight.

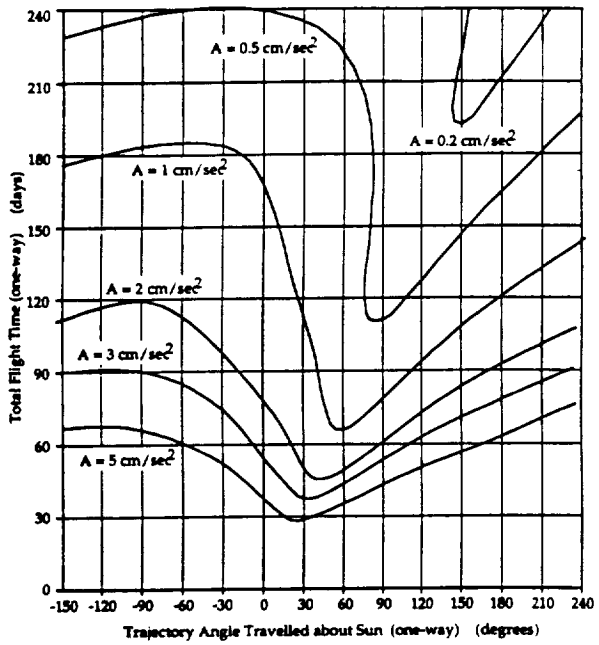

Figure 12. Flight Times vs. $\Delta\upsilon$ for constant acceleration.

Orbital Analysis Assumptions. For both the high impulse acceleration and low continuous acceleration flight startegies, the following assumptions were made:

a) orbits of the Earth and Mars are coplanar;
b) orbits of the Earth and Mars are circular with mean radii of 149.6 million km, and 227.8 million km, respectively;
c) the orbital velocities of Earth and Mars are constant and equal to the orbital velocity that would exist for the circular orbits described above;
d) parking orbits at the Earth and Mars are circular with radii of 6,700 and 3,600 km, respectively;
e) the gravitational effects of all bodies except the Earth, Sun, and Mars are neglected; and,
f) the gravitational attraction of the Earth, Sun, and Mars are treated as point sources.

General Mission Characteristics. For all computed missions for all five propulsion systems, the flight time outbound to Mars was identical to the flight time for the return from Mars. Flight times one-way were set at 240 days, 210 days, 180 days, 150 days, 120 days, and 90 days. Missions for the Chemical and two NTR systems then consisted of trajectories chosen along the lines of constant flight times shown in Figure 11 corresponding to the flight times in 30-day increments from 240 days to 90 days (see Figure 11). Likewise, for NEP and MFPS, trajectories were chosen from the lines of constant flight times from Figure 12 in 30-day increments (see Figure 12).

Results of IMLEO, Flight Time, and Launch Opportunities Comparisons.

An adequate number of missions were computed from flight trajectories represented in Figures 11 and 12, to create the plots shown in Figures 13, 14, 15, 16, 17, and 18 for flights each way to and from Mars of 240-day, 210-day, 180-day, 150-day, 120-day, and 90-day durations, respectively. Figures 13 through 18 each show a set of curves, where each curve represents the set of points defining the minimum IMLEO required for each respective stay time at Mars (ranging along the x-axis of each plot) for the propulsion systems. 'Stay time' at Mars is defined as the time interval during the mission between arrival at Low Mars Orbit (LMO) from Earth, and departure from LMO to Earth. The 'stay time' along the x-axis of the figures ranges from zero to 780 days because that is the approximate period of the relative motions of Earth and Mars in their respective orbits about the Sun. For example, approximately every 780 days the Earth and Mars go through conjunction.

Mission Flexibility. Not only do Figures 13 through 18 give an illustration of the required IMLEOs for the various propulsion systems and flight times, but mission flexibility is also indicated. The time scale used along the x-axis of Figures 13 through 18 can be used to measure the following mission parameters:

1) the time allowed at Mars, and,
2) the time duration of the window to launch from Mars for the return flight to Earth.

As an example of the parameters regarding mission flexibility, the reader is referred to Figure 17, and in particular the line of constant IMLEO on the plot equal to 1,250 metric tons. For the generic space vehicle described earlier and incorporating the MFPS with a total vehicle IMLEO of 1,250 metric tons, the time allowed at Mars with a one-way flight time of 120 days is unlimited. In other words, the vehicle could leave Mars for Earth at any time. This is indicated by the line of IMLEO=1,250 metric tons being above the MFPS' minimum IMLEO curve throughout the time scale of zero to 780 days. The line of 1,250 metric tons IMLEO also intercepts the curve for a theoretical NTR gas-core vehicle at two points. The distance between

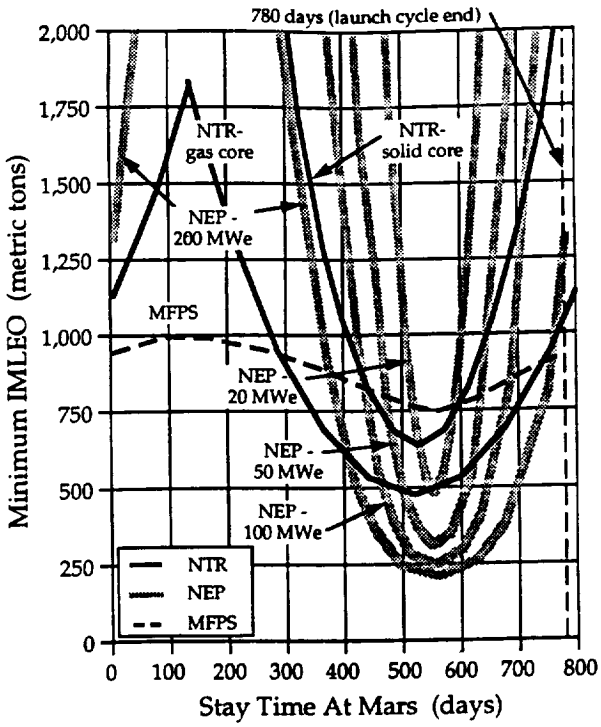

Figure 13. Required System IMLEO for 240-day flights to and from Mars.

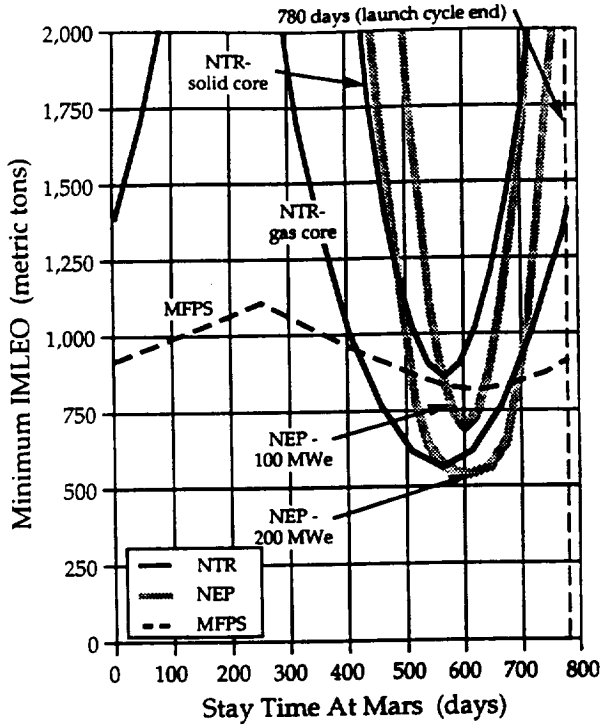

Figure 15. Required System IMLEO for 180-day flights to and from Mars.

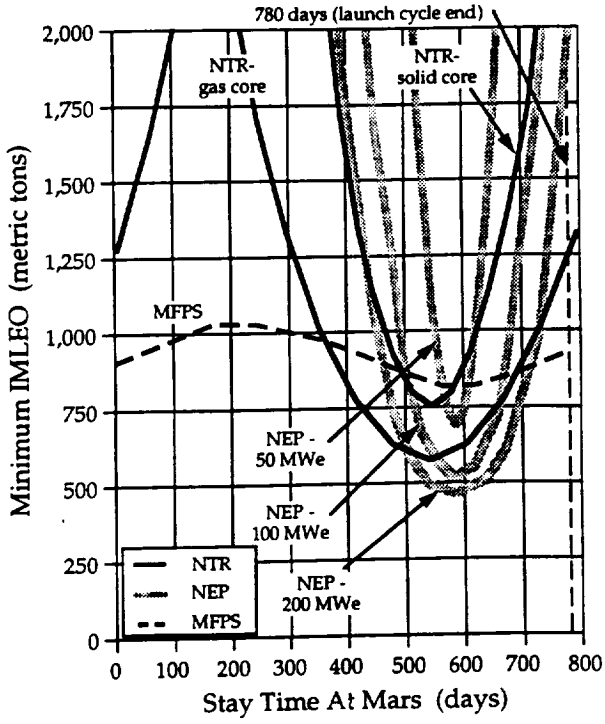

Figure 14. Required System IMLEO for 210-day flights to and from Mars.

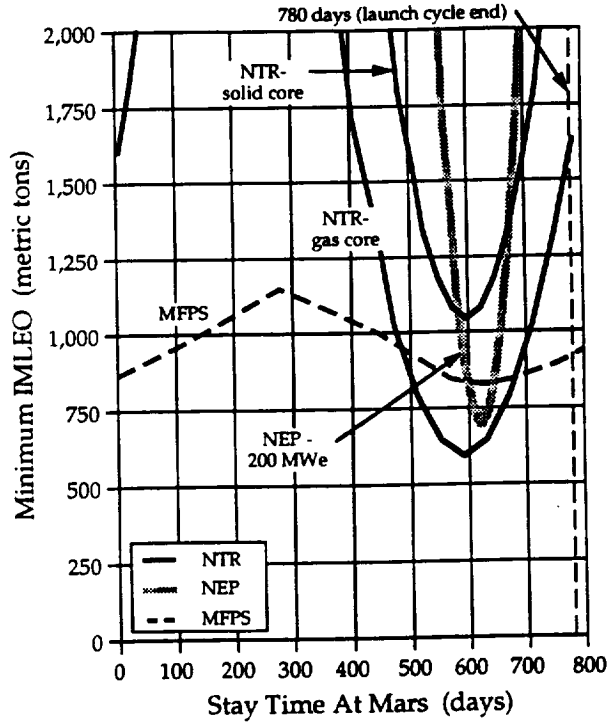

Figure 16. Required System IMLEO for 150-day flights to and from Mars.

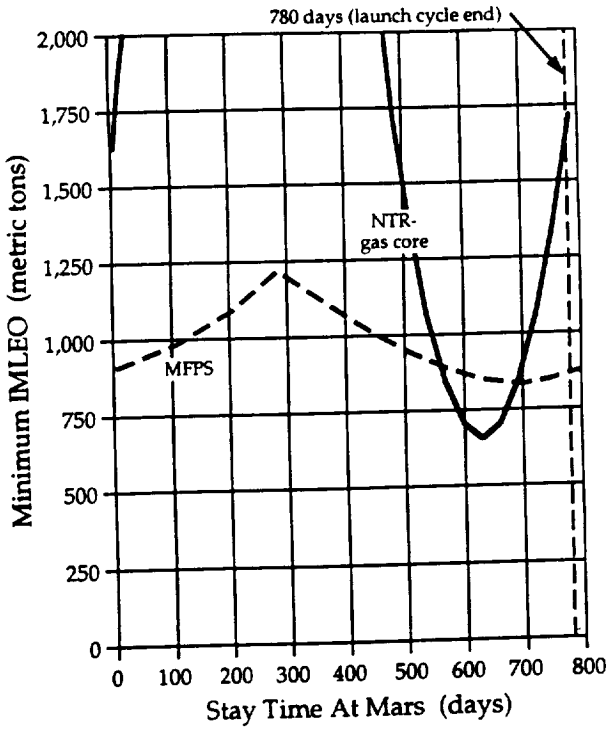

Figure 17. Required System IMLEO for 120-day flights to and from Mars.

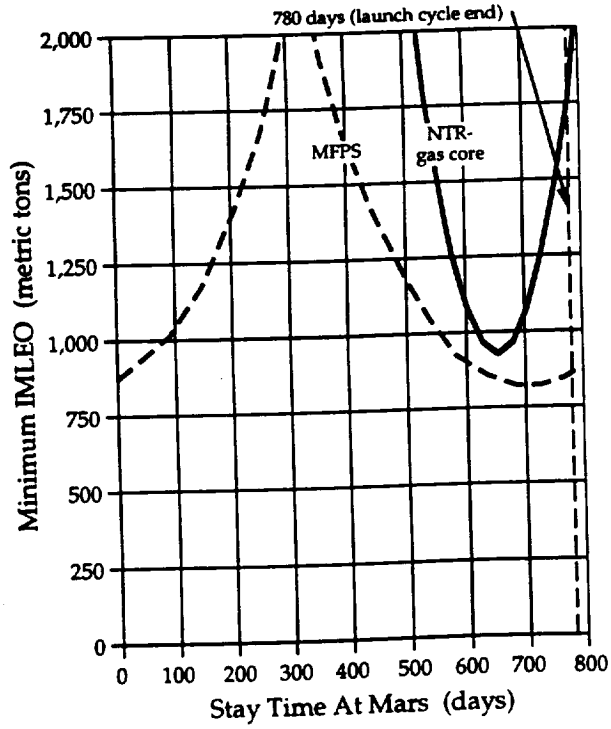

Figure 18. Required System IMLEO for 90-day flights to and from Mars.

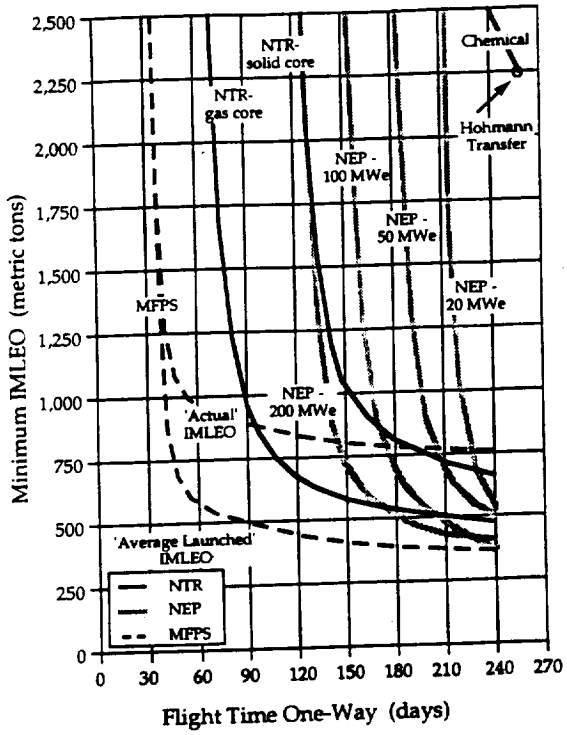

Figure 19. Minimum IMLEO versus Flight Time for Each Propulsion System and Vehicle.

the two points along the line of IMLEO=1,250 metric tons is approximately 180 days (the difference between 520 and 700 days stay time). Therefore, the NTR gas-core vehicle at an IMLEO of 1,250 metric tons, has a window of opportunity of approximately 180 days to launch from Mars to return to Earth, for a 120-day flight duration. For the NTR gas-core vehicle in this case, though, the window for return does not open until the vehicle has been in the vicinity of Mars for 520 days. In contrast, the MFPS-powered vehicle at 1,250 metric tons could leave for Earth after only 30 days, or 90 days, i.e. at any time.

Each curve in Figures 13 through 18 generally has a 'V', or quasi-parabolic shape. A common trait of all curves is that the distance between the two points of intersection on a curve for a particular line of IMLEO is shorter the closer the IMLEO line is to the curve's absolute minimum IMLEO. Again, using the NTR gas-core vehicle curve in Figure 17, the launch window for return to Earth from Mars for the vehicle absolute minimum IMLEO of 670 metric tons, is a single day, i.e. the vehicle must leave after being at Mars for approximately 610 days. If IMLEO was 750 metric tons where more propellant was on-board, as the constant IMLEO line shows in the plot, then the launch window widens to 70 days, at stay times at Mars between 575 days and 645 days. The trend for each curve, then, is for increased launch window duration for an increase in IMLEO for each flight time.

Propulsion System Performance. From Figures 13 through 18, one can see that the Chemical system is not even represented in the IMLEO range of less than 2,000 metric tons, and flight times of 240 days or less. The NTR solid-core, and NEP systems have curves in the plots represented by 240-day flight times down to 150-day flight times, though with decreasing flight times, the IMLEOs increase and launch windows narrow. The NTR gas-core system at 240-day flight times also shows unlimited launch opportunity from Mars for IMLEOs greater than 1,750 metric tons. The launch windows decrease and IMLEOs increase as flight times decrease. However, unlike most other systems, the NTR gas-core system can still support flight times of 120 days and 90 days, though with limited launch windows and larger IMLEOs. The MFPS shows unlimited mission flexibility for flight times down to 120 days, with minimum IMLEOs between 800 and 1,200 metric tons. Only when flight times decrease to 90 days does the MFPS' launch window begin to narrow, and stay times at Mars become limited.

The curves in Figure 19 are derived from the data in Figures 13 through 18. The point of absolute minimum IMLEO for each system curve for each flight time in Figures 13 through 18 was combined to form curves of absolute minimum IMLEO versus flight times in Figure 19. The maximum IMLEO values were carried out to 2,500 metric tons so that the Chemical system could be compared to the other systems.

'Actual' IMLEO versus 'Average Launched' IMLEO. All curves of the MFPS system minimum IMLEO in Figure 13 through 18 use the vehicle's 'actual' IMLEO. The actual IMLEO is the total mass of the vehicle at the start of any given mission, i.e. it is the usual definition of IMLEO. Likewise, in Figure 19, the actual IMLEOs are shown, but with one addition. For the MFPS, the curve for 'average launched' IMLEO is also shown. Average launched IMLEO is the average mass launched to LEO from Earth over many missions. The difference between actual IMLEO and average launched IMLEO can be significant if ship components are massive, and yet to be used for several missions. With the MFPS, the 460-metric-ton engine is used for eight missions. Thus, the difference between actual and average launched IMLEO is about 400 metric tons. The actual IMLEO and average launched IMLEO are both shown for MFPS in Figure 19. The 'average' engine mass of MFPS launched from Earth is then only 57,500 kg (460,000/8 kg).

The Shallow MFPS Curve. The absolute minimum for all curves in Figures 13 through 16 are all roughly in the same area of stay times of 500 to 700 days. However, the curves for MFPS in Figures 13 through 16 are 'shallower' than the other systems' curves, and the MFPS curve's minimum point is much higher on some of the plots than the minimum points of other system curves. The higher minimum point of the MFPS curve in Figures 13 through 16 is due to the large mass of the engine (460 metric tons). The MFPS engine is a large contributor to overall MFPS vehicle IMLEO. The minimum points in all curves result from missions where the Earth and Mars are favorably aligned to minimize propellant. As the positions of Earth and Mars diverge from this favorable alignment, space vehicles pay a penalty in greater propellant masses. However, the MFPS engine, though more massive, is also more efficient (specific impulse 37,000 sec), so the propellant penalties are less severe. For example, in Figure 17, the NTR gas-core system IMLEO triples when shifting stay time at Mars from a minimum of 610 days (at a corresponding 660 metric tons IMLEO) to 480 days (at a corresponding 2,000 metric tons IMLEO). However, the MFPS IMLEO only increases about 50% when the required stay time on Mars for the mission shifts from 700 days (at a corresponding 820 metric tons IMLEO) to 300 days (at a corresponding 1,220 metric tons IMLEO).

Conclusions

The MFPS is a well-characterized and studied system offering potential significant increases in mission performance for manned Mars missions. Although the engine is large (460,000 kg), it can be re-used up to 8 times resulting in an 'average' engine mass of 57,500 kg equivalent launched for each mission.

As shown in Figures 13 through 18, the MFPS has by far the greatest mission flexibility. For flight times of 8 months all the way down to 4 months, the MFPS IMLEO is always between 800,000 kg and 1,200,000 kg regardless of when the vehicle leaves Mars. Unlimited launch windows are hence offered. Only when flight times decrease to 3 months, does MFPS mission flexibility suffer.

In comparing mission performance of the MFPS to other systems, the following observations are made:

1) For longer flight times on the order of 7 or 8 months, the higher power (100 and 200 MWe) NEP systems offer the lowest actual IMLEO if stay times at Mars of 500 to 700 days are desired (see Figures 13 and 14). However, with these long flight times, crew safety is not improved, and the reactor size for this system approaches 1 GWt.

2) As flight times decrease to 5 or 6 months (Figures 15 and 16), the lower-power NEPs increase in IMLEO to greater than 2,000 metric tons. The NTR gas-core system has the least IMLEO (for stay times of 500 to 700 days).

3) At 4 month flight times, the NTR gas-core system remains competitive with the MFPS in the 550-day to 650-day stay time area. MFPS IMLEO ranges from 800 to 1,200 metric tons throughout the entire mission envelope, however.

4) Referring to Figure 19, it can be seen that the MFPS is competitive with other propulsion systems if 6 to 8 month flight times are acceptable. However, if

flight times of 90 days are desired, the MFPS is the only choice in this analysis that will support such a mission.

5) The MFPS can support the first manned missions to Mars very elegantly if short stay times are desired. Referring to Figures 16, 17, and 18, the MFPS, with an IMLEO of only about 900 to 1,000 metric tons, can support flights of only 90- to 150-day duration to and from Mars, while stay times at Mars can be less than 100 days.

In summary, the MFPS offers the shortest flight times, coupled with lower IMLEOs and total mission flexibility, then any system considered here. If crew safety and recurring cost are indeed the most important factors for the design of a Mars Transportation System, then the cost to develop the MFPS may well be worth the investment.

References

1. America on the Threshold: Report of the Synthesis Group on America's Space Exploration Initiative; U.S. Government Printing Office, 1991.
2. Carpenter, S.; Deveny, M.; Mirror Fusion Propulsion System (MFPS): An Option for the Space Exploration Initiative (SEI); IAF-92-0613; August 1992.
3 Englert, G. W.; "Toward Thermonuclear Rocket Propulsion," New Scientist 16, #307, 16 (1962).
4. Wittenberg, L. J.; Cameron, E. N.; Kulcinski, G. L.; Ott, S. H.; Santarius, J. F.; Sviatoslavsky, G. I.; Sviatoslavsky, I. N.; and Thompson, H.E.; A Review of ^{3}He Resources and Acquisition for Use as Fusion Fuel; Fusion Technology, 21, July 1992.
5. Kulcinski, G. L. and Schmitt, H. H.; Fusion Power from Lunar Resources; Fusion Technology, 21, July 1992.
6. Emmert, G. A., El-Guebaly, L., (et. al.); Possibilities for Breakeven and Ignition of D-^{3}He Fusion Fuel in a Near Term Tokamak; Nuclear Fusion, Vol. 29, No. 9 (1989).
7. Emmert, G. A. and Parker, R.; Potential for D-^{3}He Experiments in Next-Generation Tokamaks; Fusion Technology, 21, July 1992.
8. Orth, C.D., Klein, G., Sercel, J., Hoffman, N., Murry, K., and Chang-Diaz, F.; VISTA: A Vehicle for Interplanetary Space Transport Applications Powered by Inertial Confinement Fusion; LLNL, UCRL-53802 (1987).
9. R. W. Bussard; Fusion as Electric Propulsion; J. Propulsion, Vol. 6, No. 5, Sept.-Oct. 1990.
10. Cristofilos, N.C.; Trapping and Lifetime of Charged Particles in the Geomagnetic Field; UCRL-5407, November 28, 1958.
11. Post, R.F.; Summary of UCRL Pyrotron (Mirror Machine) Program, UCRL-5044, June 27, 1958.
12. Post, R.F.; Summary of the LRL Mirror Machine Program, 1958-60; UCRL-6533, August, 1961.
13. Post, R.F.; a paper presented at the "Classified Conference on Thermonuclear Reactors held at Denver on June 28, 1952," U.S. Atomic Energy Commission, Technical Information Service, Oak Ridge, Tenn., Report No. WASH-115, December, 1952.
14. Dimov, G. I., Zakaidakov, V. V., and Kishinevskii, M. E. (1976). *Fiz. Plasmy* 2, 597 [*English transl.: Sov. J. Plasma Phys.* 2, 326-333].
15. Fowler, T. K., and Logan, B. G. (1977). *Comments Plasma Phys. Controlled Fusion Res.* 2, 167-172.
16. Moir, R. W., and Post, R. F. (1969), *Nucl. Fusion* 9, 253-258.
17. Moir, R.W., et. al.; Preliminary Design Study of the Tandem Mirror Reactor (TMR); UCRL-52302, Lawrence Livermore National Laboratory (LLNL), July 15, 1977.
18. Baldwin, D. E., and Logan, B. G. (1979), Phys. Rev. Lett. 43, 1318-1321.
19. Porter, G.D., Ed.; TMX-U Final Report; UCID-20981, Vol. 1 & 2, February 1, 1988.
20. MARS: Mirror Advanced Reactor Study Final Report; LLNL, UCRL-53480 (1984).
21. Hooper, E.B., Jr.; Octopole Anchor for Tandem Mirrors; UCID-20050, March 21, 1984, LLNL.
22. MINIMARS Conceptual Design: Final Report; J.D. Lee Ed.; UCID-20773, Vol. 1, September 1986.
23. McNally, J. R. Jr.; Fusion Reactivity Graphs and Tables for Charged Particle Reactions; ORNL/TM-6914 (1979).
24. Howerton, R. J., UCRL-50400, Vol. 21, Pt. A; LLNL (1979).
25. McCool, S. C., Edmonds, P. H., and Castle, G. G.; An Assessment of the Feasibility of Fueling a Tokamak Reactor with Lithium Titride Pellets; Fusion Technology, Vol. 21, 1992.
26. McNally, J. R. Jr., Physics of Fusion Fuel Cycles; Nuclear Technology/Fusion, Vol. 2 (1982).
27. Fidone, I., Granata, G., Giruzzi, G., and Mazzucato, E.; Synchrotron Radiation Loss in a Tokamak Reactor in the Presence of an Enhanced Electron Trail; Nuclear Fusion, Vol. 31, No. 11 (1991).
28. Xing-Zhong Li, Kesner, J., and LoDestro, L. L.; Wall Stabilized High Beta Mirror Plasma in a Rippled Magnetic Field; Nuclear Fusion, Vol. 27, No. 8 (1987).
29. Xing-Zhong Li, Kesner, J., Lane, B.; MHD Stabilization of a High Beta Mirror Plasma Partially Enclosed by a Conducting Wall; Nuclear Fusion, Vol. 27, No. 1 (1987).
30. Kumakura, H.; Togano, K.; Kase, J.; Morimoto, T.; and Maeda, H.; Superconducting Properties of textured Bi-Sr-Ca-Cu-O Tapes Prepared by Applying Doctor Blade Casting; in Cryogenics 1990, Vol. 30, November.
31. P. Haldar, J. G. Hoehn, Jr., J. A. Rice, M. S. Walker, and L. R. Motowidlo; Transport Critical Current Densities of Silver Clad Bi-Pb-Sr-Ca-Cu-O Tapes at Liquid Helium and Hydrogen Temperatures; Appl. Phys. Lett. 61 (5), 3 August 1992.
32. Collings, E. W.; Conductor Design with High-Tc Ceramics: A Review; in Advances in Superconductivity-II, Proceedings of the 2nd International Symposium on Superconductivity, (ISS '89), November 14-17, (1989) Tsukuba.
33. F.M. Sauerzopf, H.P. Wiesinger, H.W. Weber, and G.W. Crabtree; Neutron Irradiation Effects on YBCO Single Crystals; Advances in Cryogenic Engineering (Materials), Vol. 38, 1992.
34. LoDestro, L.L.; Private communication, August 26, '92.
35. Pekala, R.W.; Alviso, C.T.; Carbon Aerogels and Xerogels; submitted to Materials Research Society, 1992 Spring Meeting, San Francisco, CA, April 1992.

36. Hawke, R. S.; Devices for Launching 0.1-g Projectiles to 150 km/s or More to Initiate Fusion, Part 2, Railgun Accelerators; UCRL-52778 Part 2, LLNL, 1979.
37. Hawke, R. S.; Fusion Fuel Pellet Injection with a Railgun; J. Vac. Sci. Technol. A 1 (2), Apr.-June 1983.
38. Post, R.F.; Private communication; July, 13, 1992.
39. Fowler, T. K.; Private communication, July 10, 1992.
40. Kunkel, W. B.; Neutral-Beam Injection; in *Fusion*, Teller, E. Ed.; Vol. 1, Part B; Acedemic Press (1981).
41. McDanels, D. L., Baker, K. W., Ellis, D. L., Graphite Fiber/Copper Matrix Composites for Space Power Heat Pipe Fin Applications; American Institute of Physics (1991), CONF-910116.
42. Mensing, A.E.; Latham, T.S.; Gas-core Technology; Aerospace America; June 1989.
43. Seigfried, W.; The Space Exploration Initiative: An Industry Team's Perspective, McDonnell Douglas Space Systems Co., 1990.
44. Space Nuclear Power Systems, Part 2; 8th Symposium; Albuquerque, NM; 1991.
45. Kaplan, M. H.; Modern Spacecraft Dynamics & Control; John Wiley & Sons; 1976.
46. Bate, R. R., Mueller, D. D.; White, J. E.; Fundamentals of Astrodynamics; Dover Publications; 1971.
47. Tsien, H.S.; "Takeoff from Satellite Orbits", Journal of the American Rocket Society, July-August, 1953.
48. Stuhlinger, E.; Ion Propulsion for Space Flight; NASA, McGraw Hill Book Co., 1964.
49. Irving, J.H; Low Thrust Flight: Variable Exhaust Velocity In Gravitational Fields; Chapter 10 in Space Technology, John Wiley and Sons, 1959.
50. Deveny, M.; Characterization of Trajectories Between Earth and Mars Using Continuous Accelerations of 10^{-4} to 10^{-2} G's; unpublished paper, 1993.